Supplementary Information

$Ti_3C_2T_x$-MXene/PET textile-based Flexible Pressure Sensor for Wearable Pulse Monitoring

Qingchao Zhang[1], Huinan Zhang[1], Jie Liang[1], Xuefeng Zhao[2], Bo Li[3], Junbin Zang[1], Libo Gao[4], Zhidong Zhang[1], and Chenyang Xue[1]*

1. Key Laboratory of Instrumentation Science & Dynamic Measurement of Ministry of Education, North University of China, Taiyuan 030051, China
2. State Key Laboratory of High Performance Ceramics and Superfine Microstructure, Shanghai Institute of Ceramics, Chinese Academy of Sciences, Shanghai 200050, China
3. School of Software, North University of China, Taiyuan 030051, China
4. Pen-Tung Sah Institute of Micro-Nano Science and Technology, Xiamen University, Xiamen, 361102, China

* Corresponding author. E-mail: zdzhang@nuc.edu.cn (Z. Zhang)

Total number of figures: 19 (Figure S1-S19)

Total number of tables: 2 (Table S1-S2)

Total number of texts: 2 (Text S1-S2)

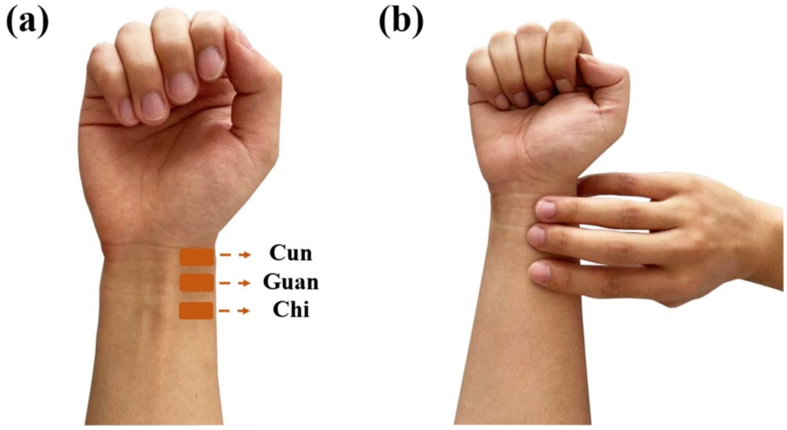

Figure S1. (a) Schematic diagram of the three parts of Cun, Guan and Chi. (b) Pulse diagnosis in Chinese medicine

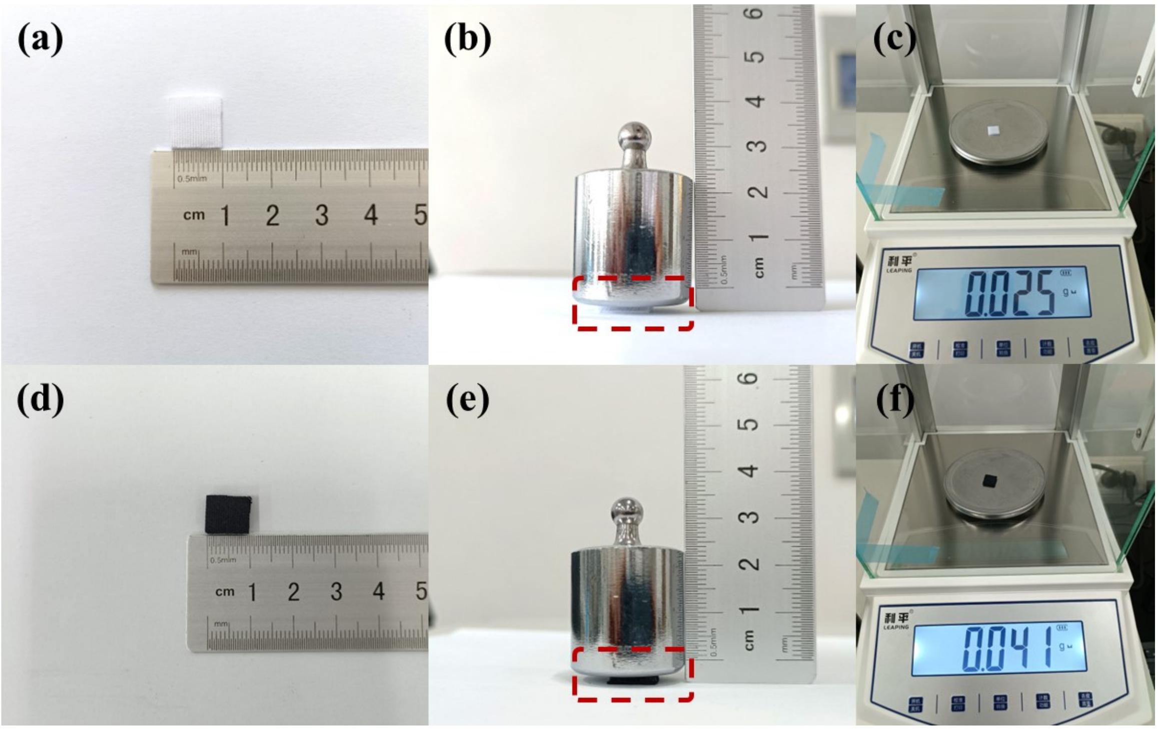

Figure S2. (a) Physical image of the textile before impregnation. (b) Schematic diagram of textile under 100g weights before impregnation. (c) Weight of the textile before impregnation. (d) Physical image of the textile after impregnation. (b) Schematic diagram of textile under 100g weights after impregnation. (c) Weight of the textile after impregnation.

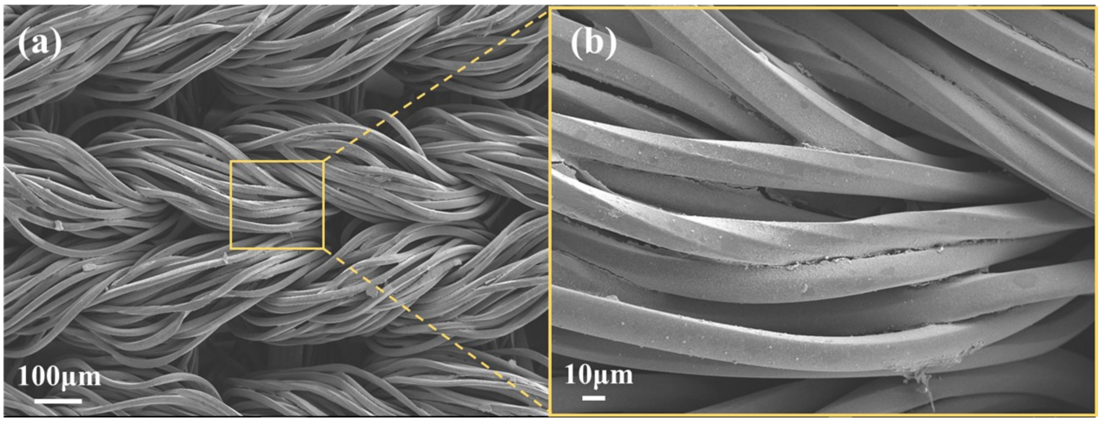

Figure S3. (a) Yarn structure of the plain knit fabric. (b) Localized enlarged image of the yarn.

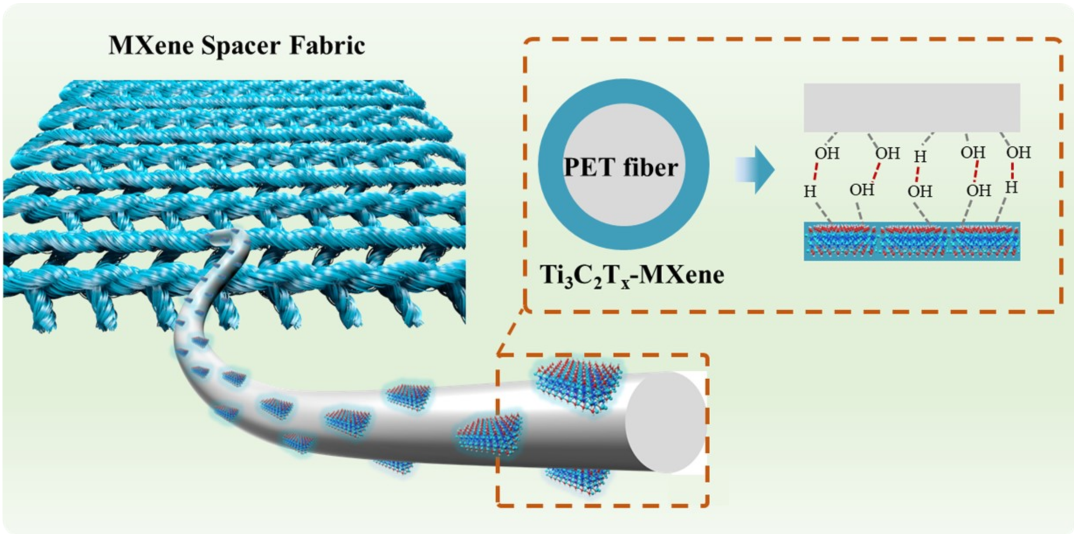

Figure S4. Schematic diagram of the interaction between fiber and $Ti_3C_2T_x$-MXene.

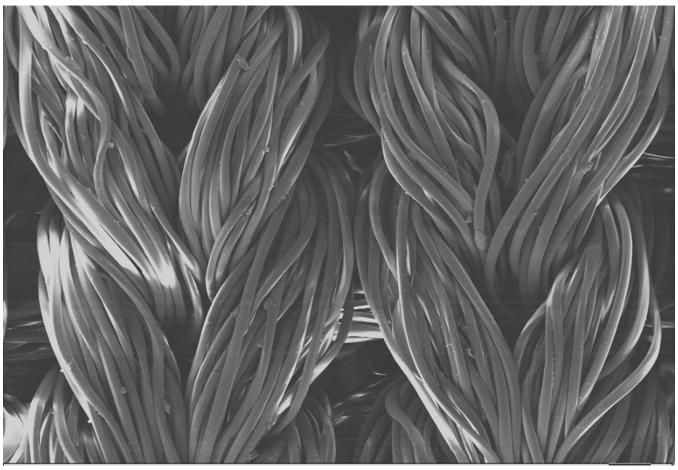

Figure S5. SEM image of unimpregnated textile.

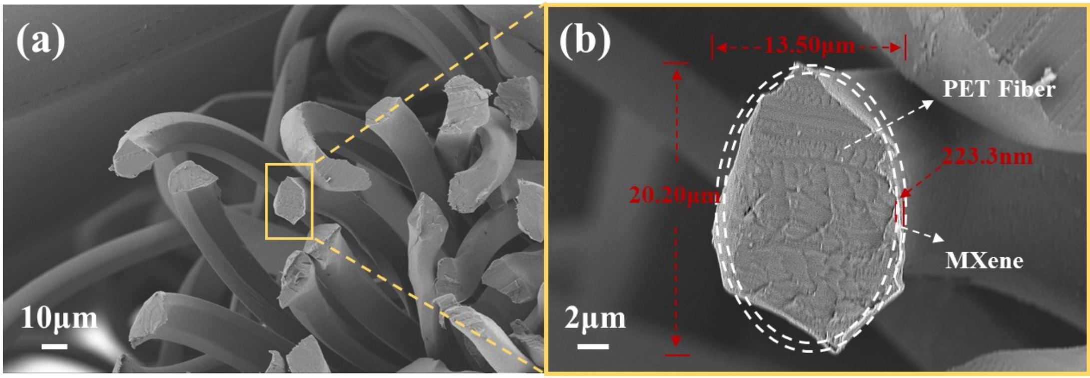

Figure S6. (a) Fiber cross-section after impregnation. (b) Fiber diameter and impregnation thickness.

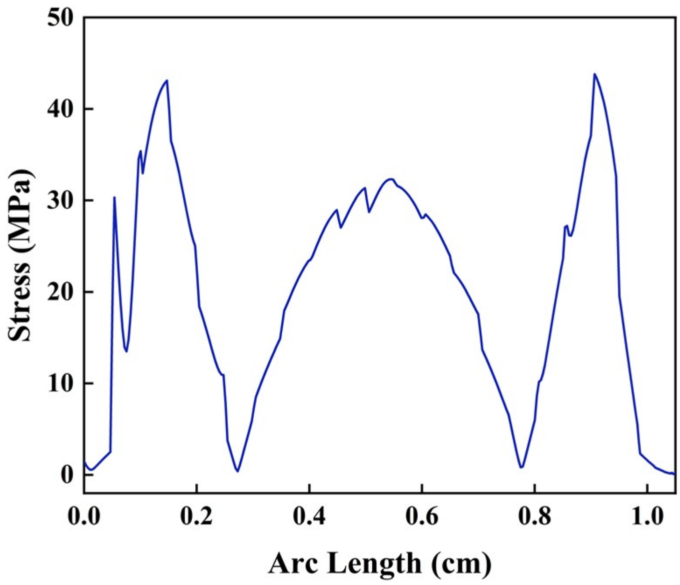

Figure S7. The stress curve along the supporting fiber.

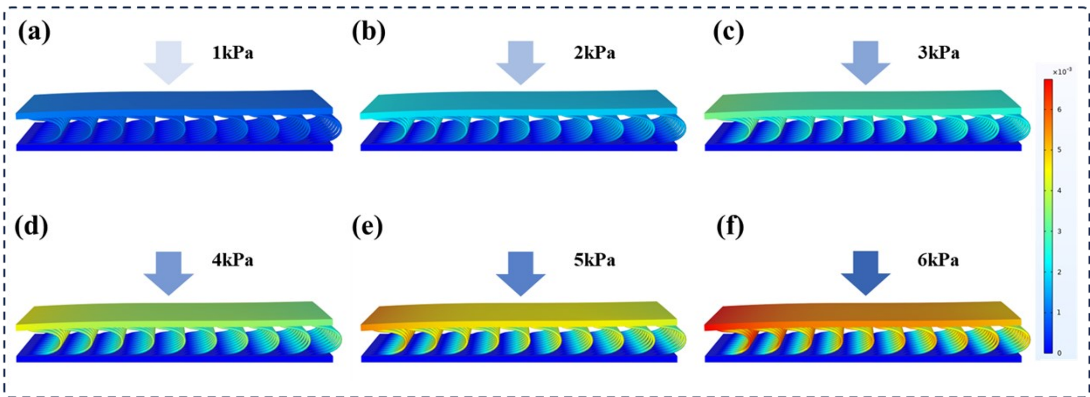

Figure S8. Displacement distribution of textiles at 1-6 kPa.

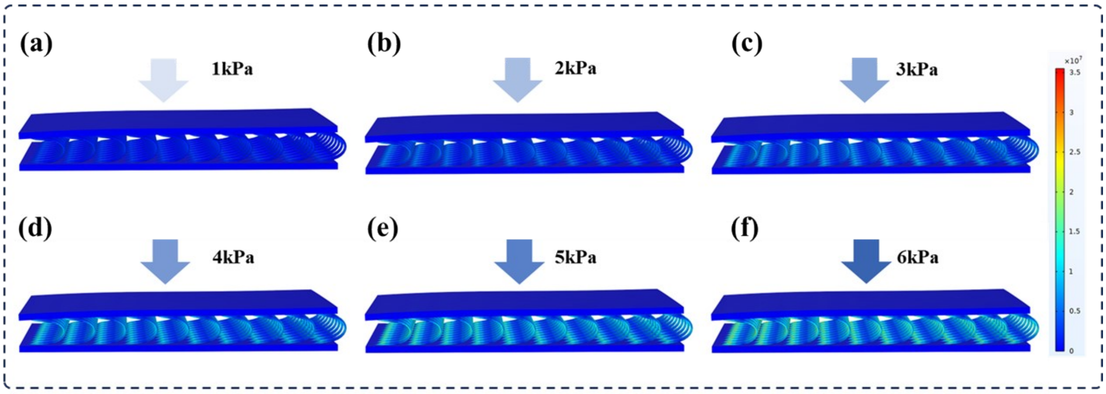

Figure S9. Stress distribution in textiles at 1-6 kPa

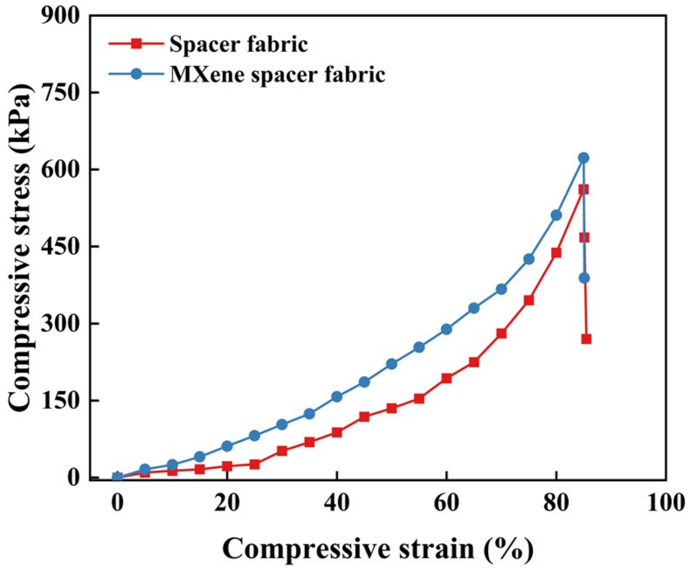

Figure S10. Compression stress–strain curves for spacer fabric and $Ti_3C_2T_x$-MXene spacer fabric.

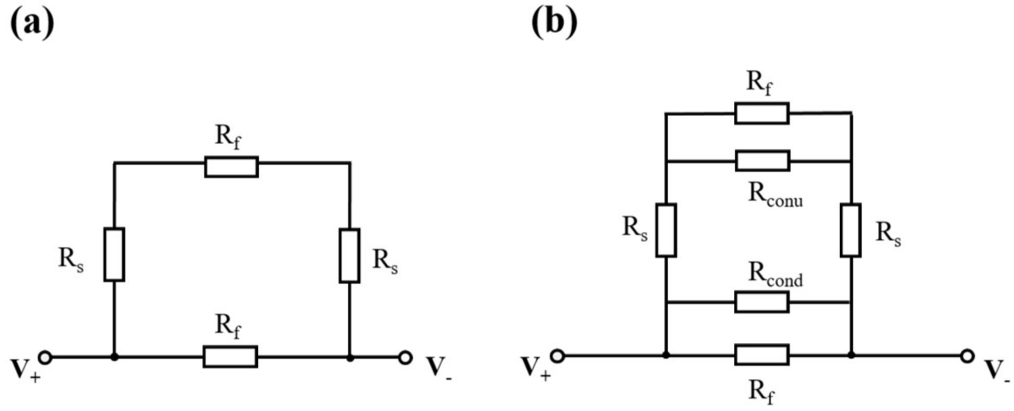

Figure S11. (a) Equivalent circuit in the initial state. (b) Equivalent circuit under pressure.

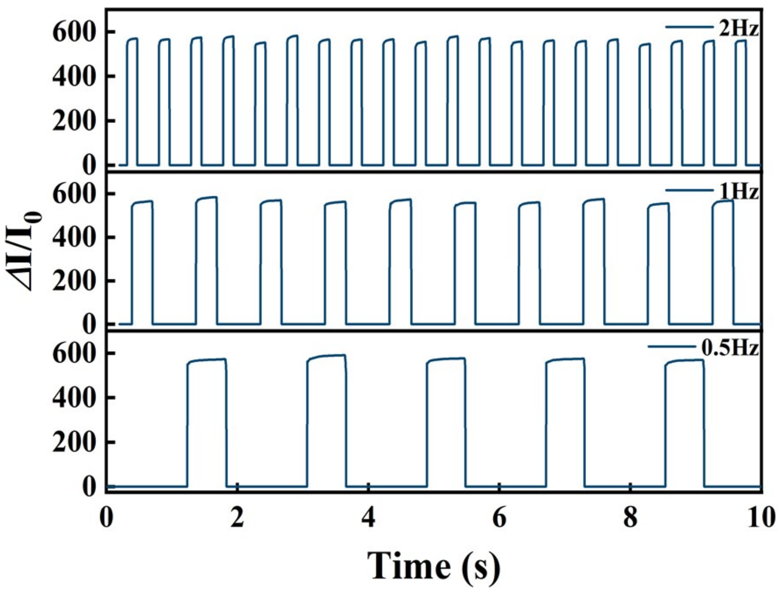

Figure S12. The frequency response performance of the MSF sensor under 15kPa.

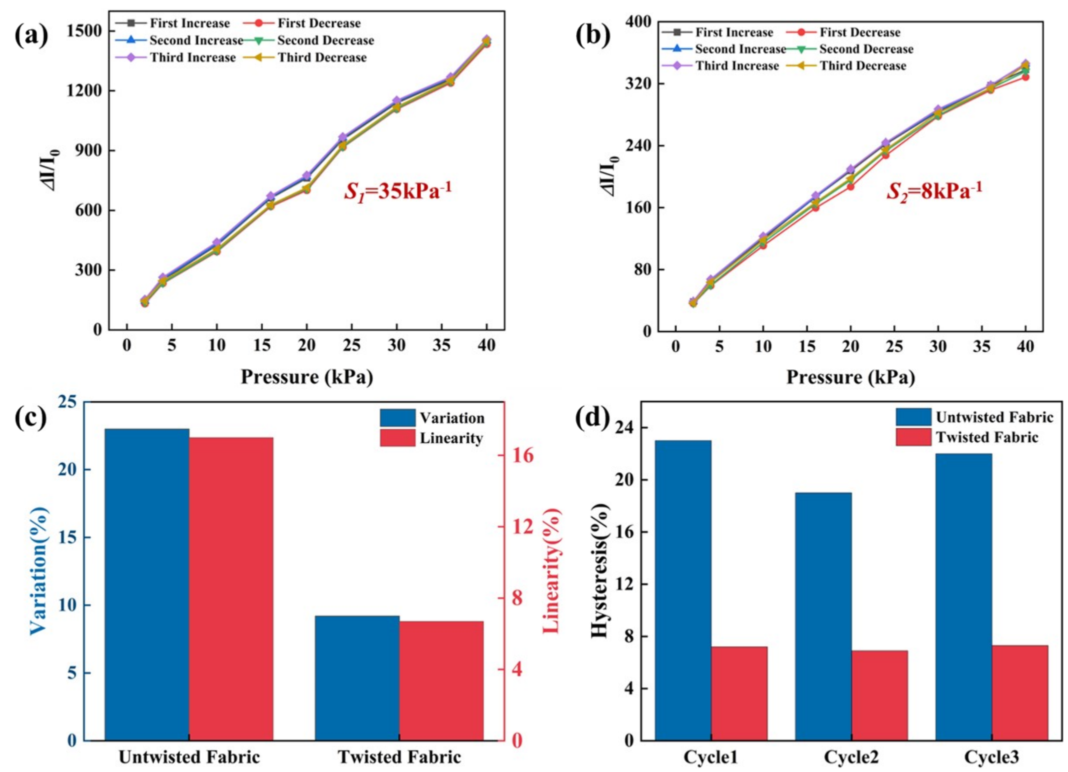

Figure S13. Textile sensor properties with twisted/untwisted yarns. (a)-(b) Three loading–unloading transfer curves of textile sensors made from twisted yarns and untwisted yarns were recorded at a pressure of 40 kPa. (c) A comparison of variation and linearity for textile sensors with/without twisted yarns. (d) The hysteresis of three cycles.

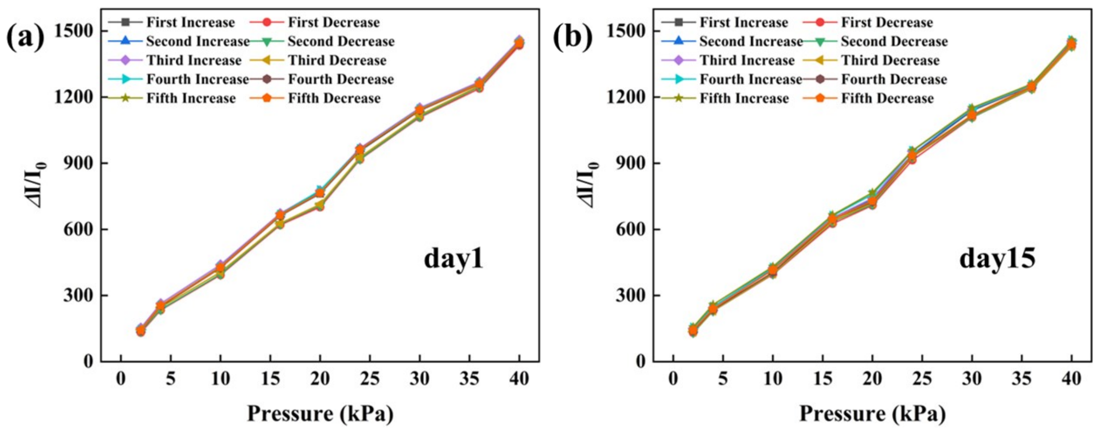

Figure S14. The output current for five increases and decreases pressure cycles.

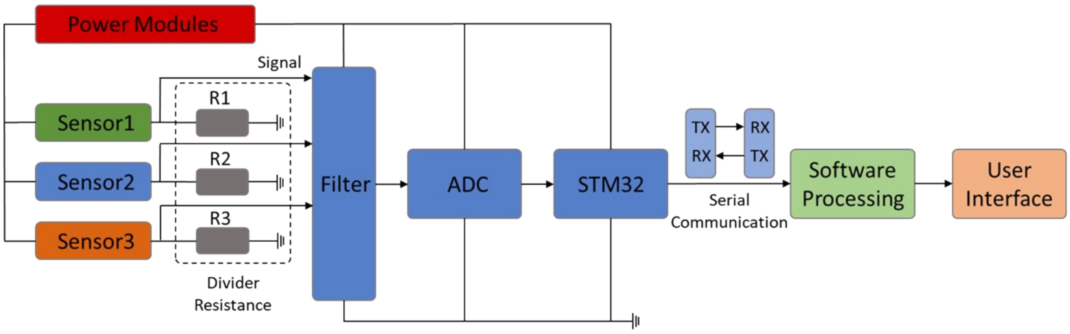

Figure S15. Pulse signal acquisition system hardware circuit structure diagram.

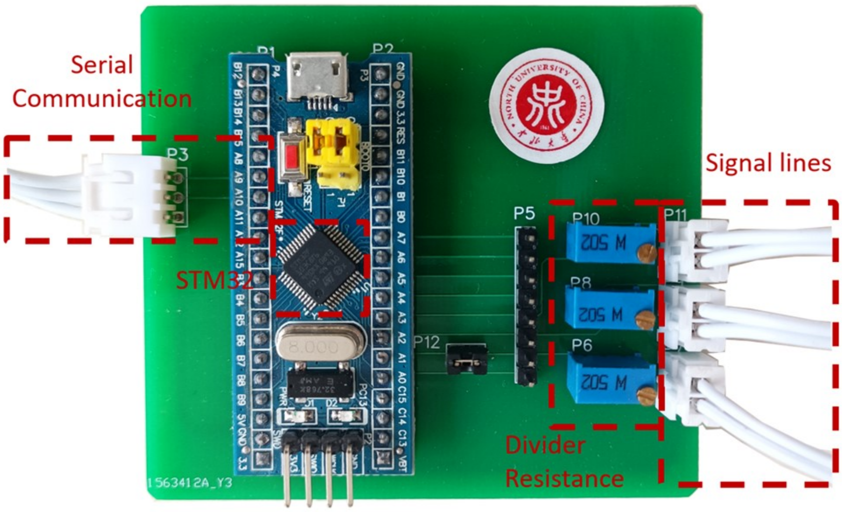

Figure S16. Physical image of the hardware circuit.

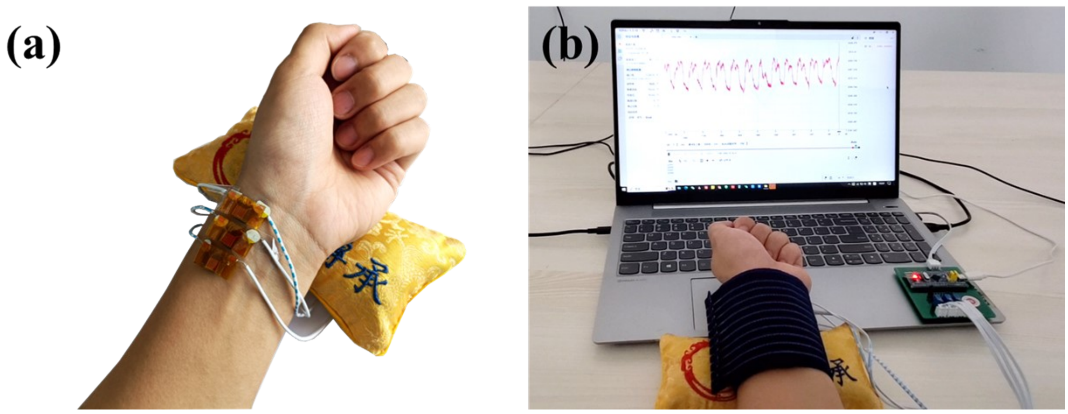

Figure S17. (a) Triple sensor array. (b) Pulse signal acquisition system.

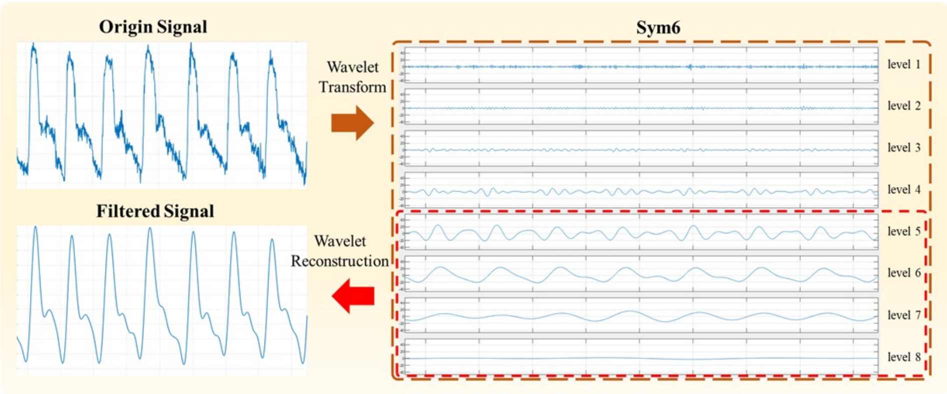

Figure S18. The structure of pulse signal filtering using wavelet decomposition.

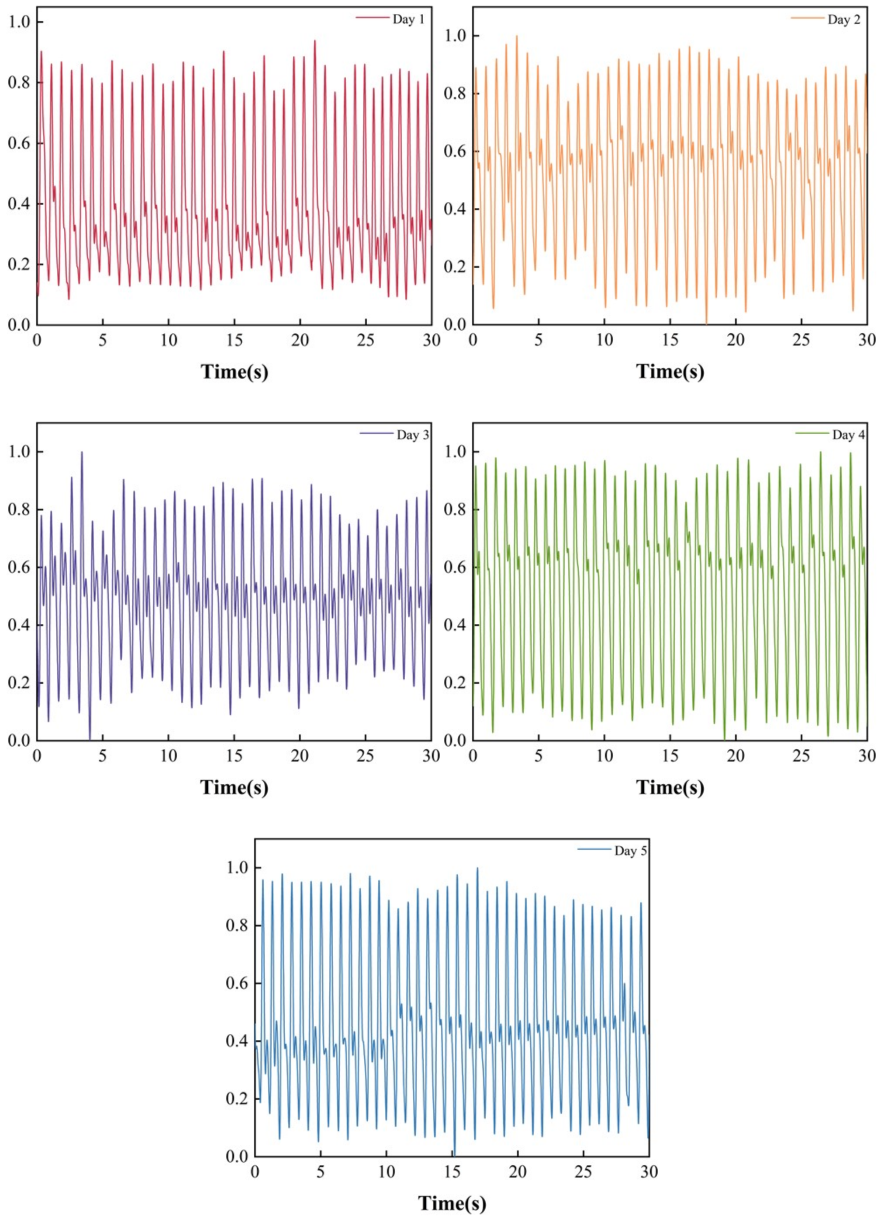

Figure S19. Pulse waveform of an influenza patient with fever for five days.

Table S1. Performance comparison of pressure sensors based on textile structures.

Structure	Materials	Sensitivity (kPa^{-1})	Sensing range (kPa)	Response time (ms)	Recovery time (ms)	Cycle stability (10^3 times)	Ref
3D	**MXene/PET**	**35**	**0-40**	**15**	**15**	**2**	**This**
3D	Carbonized Cellulose Fabric	32.13	0-3	81	78	50	35
		1.18	3-20				
3D	Nickel/Space Fabric	0.042	0-6			10	19
		0.330	6-21				
		0.037	21-110				
2D	MXene/NWF	6.31	0-150	300	260	12	22
2D	MXene/PPy	20.1	0-2	100	80	1	23
		0.6	2-25				
		0.16	25-80				
2D	MXene@SiNPs/Cotton	12.23	0-13				24
		2	13-52				
		8.46	52-80				
2D	MXene/Textile	3.844	0-29	26		5.6	36
		12.095	29-40				
2D	MXene/Textile	19.78	0-0.5	149	139	10	37
		6.11	0.5-2				
		1.61	2-5				

Table S2. List of feature extraction based on the pulse signal.

Feature Set	No.	Index	Definition
Time-domain Feature (TF)	1	PT	Period Time
	2	PR	Pulse Rate
	3	PPT	Time from P_1 to P_3
	4	AT	Ascending Time
	5	DT	Descending Time
Waveform Feature (WF)	1	AI_r	Augmentation Index
	2	AS	Ascending Slope
	3	DS	Descending Slope
	4	AA	Ascending Area
	5	DA	Descending Area

Text S1: The calculation process of the variation, hysteresis, and linearity.

To evaluate the sensor performance, the variation (*Var*), hysteresis (*Hys*), and linearity (*Lin*) were defined as:

$$Var = \frac{\delta_{1\_max}}{I_{F.S.}} \times 100\% \tag{S1}$$

$$Hys = \frac{\Delta_{FC\_BC}}{I_{F.S.}} \times 100\% \tag{S2}$$

$$Lin = \frac{\Delta_{FC\_Fit}}{I_{F.S.}} \times 100\% \tag{S3}$$

Where δ_{1_max} is the maximum deviation of output current to show the repeatability error in the whole calibration region and $I_{F.S.}$ is the full-scale current output. Δ_{FC_BC} is the maximum difference between increase and decrease transfer curves. Δ_{FC_Fit} is the maximum deviation of output current, which is considered as the error in the linear fitting region.

Text S2: Detailed description of wavelet decomposition.

Wavelet decomposition is divided into two steps: wavelet transform and wavelet reconstruction. Wavelet transform provides a time-frequency window that can be adaptively adjusted according to signal characteristics by improving the trigonometric function in Fourier transform into a fast-decaying wavelet function. The wavelet function solves the problem that the resolution of the short-time Fourier transform is not adjustable. Wavelet transform can automatically adapt to the requirements of signal time-frequency analysis and can accurately analyze the local characteristics of the signal. According to the continuity of basis function, wavelet transform can be divided into continuous wavelet transform and discrete wavelet transform. The calculation formula of continuous wavelet transform is:

$$WT(a,\tau) = \int_{-\infty}^{+\infty} f(t) \cdot \frac{1}{\sqrt{a}} \cdot \psi^* (\frac{t-\tau}{a}) dt \tag{S4}$$

where $\psi_{a,\tau}(t)$ is the wavelet basis function, *a* is the scale factor. When $a > 1$, $\psi_{a,\tau}(t)$ stretches on the time axis; when $a < 1$, $\psi_{a,\tau}(t)$ compresses on the time axis. And τ is the translation factor, which controls the mount of translation of $\psi_{a,\tau}(t)$ on the time axis. For computational processing, the continuous wavelet needs to be made discrete to minimize redundancy, so that $a = a_0^j$, $\tau = a_0^j k$. The formula for discrete wavelet transform is:

$$DWT(j,k\tau_0) = \int_{-\infty}^{+\infty} f(x) \cdot \psi_{j,k\tau_0}^*(t) dt \tag{S5}$$

There are different wavelet functions to meet the requirements of different signals. Common wavelet basis functions are Harr wavelet, Daubechies wavelet, Coiflet wavelet, Symlets wavelet and Morlet wavelet. Among them, the Symlet function is a nearly symmetric wavelet with good regularity and the ability to avoid phase distortion. Wavelet reconstruction is to use the threshold method to process the decomposed signal containing the noise, and then reconstruct the decomposed signal to obtain the denoised signal. The process is shown in Fig. S18 (ESI†). Sym6 is selected as the wavelet function of pulse signal processing, and the original pulse signal is decomposed into eight levels. Then the wavelet reconstruction is performed on the 5-8 levels to obtain the filtered pulse signal.